Lexington Laboratories, Inc.

84 SHERMAN STREET
CAMBRIDGE, MASS. 02140
Area Code 617 • 864-5020

EVALUATION OF VAPOR DEPOSITION GROWTH OF OXIDE SINGLE CRYSTALS FROM METAL HALIDES

FINAL REPORT

by

Philip S. Schaffer
Lexington Laboratories, Inc.
Cambridge, Massachusetts 02140

Contract Number Nonr-4574(00)
ARPA Order Number 306
Project Code Number 3730

May, 1965

Office of Naval Research
Department of the Navy
Washington, D. C. 20425

EVALUATION OF VAPOR DEPOSITION GROWTH OF OXIDE SINGLE CRYSTALS FROM METAL HALIDES

FINAL REPORT

by

Philip S. Schaffer
Lexington Laboratories, Inc.
Cambridge, Massachusetts 02140

Contract Number Nonr-4574(00)
ARPA Order Number 306
Project Code Number 3730

May, 1965

Prepared for:

Office of Naval Research
Department of the Navy
Washington, D. C. 20425

BLANK PAGE

TABLE OF CONTENTS

LIST OF FIGURES

LIST OF TABLES

FOREWORD

This is the final report on"Evaluation of Vapor Deposition Growth of Oxide Single Crystals from Metal Halides" for the Office of Naval Research(ONR) under Contract Nonr-4574(00) covering the period 1 May 1964 - 30 April 1965. This research is a part of Project DEFENDER, sponsored by Advanced Research Project Agency, Department of Defense and technically monitored by the Office of Naval Research (Physical Sciences Division). The principal investigator for this contract was Philip S. Schaffer of Lexington Laboratories, Inc.

1.0 SUMMARY

A vapor phase growth technique was developed for the epitaxial growth of orien ed ruby monocrystals. Crystals were grown up to 90.7 grams in 52 hours. Detailed investigations were made to determine the variables which influenced the formation kinetics of the reaction system represented by the following equation:

$$(2-x)AlCl_3(g) + xCrCl_3(g) + 3H_2(g) + 3CO_2(g) \rightleftharpoons$$

$$Cr_xAl_{2-x}O_3(s) + 3CO(g) + 6HCl(g) \qquad (1)$$

where $x > 0$ and $x = 0$ for ruby and sapphire, respectively. These variables included substrate temperature, total pressure, orientation, reactant gas velocity and reactant gas partial pressures. Crystals were grown with total impurity levels as low as 4 ppm. Dislocation density decreased with increasing thickness of vapor overgrowth. Densities as low as $13/cm^2$ were measured on large vapor-grown α-Al_2O_3 platelets, although the vapor-grown monocrystals generally exhibited a density reduction of one to three orders of magnitude over their flame fusion substrates.

2.0 INTRODUCTION

Vapor phase deposition and epitaxial growth can be obtained when reactant gases under controlled conditions of pressure, temperature and supersaturation are passed over a heated substrate. At elevated reaction temperatures, molecules of the growth species have high mobility and tend to diffuse to preferred surface sites where molecular aggregation and growth occurs. Optimum conditions of temperature, deposition rate, nature of substrate and substrate-deposit lattice match facilitate epitaxial growth of crystals with controlled orientations, morphologies, low strain and high purities.

Ruby and sapphire single crystals have been grown by several methods; each method being subject to intrinsic limitations. In the Verneuil or flame fusion method, the resultant boules contain significant impurities, internal strains and compositional inhomogeneities. Impurity contents are related to preparation of the fine particle size feed powders. The temperature gradient at the locus of growth produces high internal strains which must be reduced by long annealing cycles. Homogeneous chromium distribution cannot be achieved due to problems of different solubilities. Lineage due to internal orientation variation, opaque layers and chromium banding are existing visual imperfections. The major advantages of the Verneuil method are that a rapid growth rate can be obtained and a crucible is not required to contain a melt.

Hydrothermal synthesis is used for ruby and sapphire growth and involves the use of aqueous solutions under moderately high temperatures and high pressures to dissolve

and redeposit materials that are relatively insoluble under ordinary conditions. These reactive solutions result in the incorporation of impurity atoms in the crystal lattice. Another limitation is that low growth rates are obtained. A major advantage is the low temperature gradient between the seed and the nutrient which results in relatively low internal strains.

Flux growth involves the use of an inorganic solvent such as an oxide or halide to obtain crystallization by slowly cooling a saturated solution. Uniform dopant concentration is difficult to obtain unless the solute is continuously replenished. Flux growth is not adaptable if the material has a high vapor pressure at the melting point, decomposes before melting, or does not exist in the desired polymorph at the melting point. Growth rates are generally low and high purity is difficult to achieve due to the nature of the solution. Relatively low internal strain can be achieved since the thermal gradient is low.

The Czochralski method necessitates the use of a crucible to contain the molten alumina which can lead to the incorporation of impurities in the resultant boule. Because of the nature of the process, residual strains due to the thermal gradients present during solidification, Cr_2O_3 inhomogeneities and bubble formation still present limitations to growth of highly perfect crystals. A major advantage to this process is the attainment of reasonably high growth rates.

3.0 LITERATURE REVIEW

Except for the work cited by Schaffer[1] on the vapor growth of sapphire monocrystals, vapor phase growth of large oxide single crystals has not been heretofore reported. He reported a vapor phase growth technique in which oriented single crystals were grown up to a weight of five grams. The technique consisted of oxidizing aluminum chloride vapor with a carbon dioxide-hydrogen mixture to form the growth species which were isothermally deposited on an oriented substrate. Etch pit studies showed a maximum of 10^4 dislocations/cm^2 and an average of $5 \times 10^3/cm^2$ on the basal plane. Total impurity levels below 40 ppm were obtained.

Jack and Stephenson[2] used a vapor modification of the flame-fusion process for growing ruby and sapphire single crystals by oxidizing or hydrolyzing a halide vapor in a burner flame to produce the desired oxide. Steady state conditions were maintained during growth by rotation of the seed and controlled withdrawal of the crystal to keep the growth surface in the same furnace position. Long annealing cycles were required to permit cutting and grinding operations without shattering the boule.

Van Houten et al.[3], coated beryllia tubes with alumina by a vapor deposition process in which aluminum chloride vapor, obtained by volatilizing solid aluminum chloride, was reacted with hydrogen and carbon dioxide gases at atmospheric pressure.

Powell et al.[4], formed thin oxide coatings up to 0.0004 inches thick by using a metal chloride and water-gas reaction. Non-adherent oxide powder was formed in increasing amounts up to 1000°C, while above 1200°C no adherent oxide coating was

obtained.

Several investigators have grown ruby and sapphire crystals by hydrothermal, flux and Czochralski methods. Battelle[5] grew ruby crystals by hydrothermal synthesis at a rate of 0.02 mm/hr at a pressure of three kilobars in a solution of 2 M Na_2CO_3 -0.2 M NH_4F. The temperature gradient between the nutrient (750°C) and the seed (600°C) was moderately low and probably produced crystals with low residual strain, although no dislocation density was reported.

White et al.[6], have grown ruby crystals hydrothermally using potassium carbonate solutions (K_2CO_3), corundum source material and potassium dichromate ($K_2Cr_2O_7$). Growth was inhibited by increasing dichromate concentrations. A flux method was also used for spontaneous nucleation in a slowly cooled saturated lead fluoride solution. Chromium doping was achieved by the addition of ammonium dichromate [$(NH_4)_2 Cr_2O_7$]. The tendency for chromium concentration to decrease toward the crystal surfaces was overcome by replenishing the chromium in solution. Hexagonal platelets were obtained up to 0.1 cm thick and 0.2 cm diameter; larger platelets contained flux inclusions.

Sapphire crystals grown by Lambdin[7] in 2-7 molal potassium carbonate solutions at pressures of 5,000-30,000 psi at a temperature range of 425-600°C had a maximum growth rate of 0.0015 in/hr and were nearly strain-free. Ruby growth studies obtained growth rates of 0.0004-.0008 in/hr at a pressure of 10,000 psi.

Miller et al.[8], have grown ruby crystals from solution in fused-salt solvents. The major obstacle encountered was the apparent cessation of growth following a period of

reasonably high crystallization rate at the beginning of each growth run. Potential causes were changing crystal morphology, solute-solvent side reaction to yield a stable mixed phase, rate of mass transport and the kinetics of the solute precipitation reaction.

Nestor[9] has utilized the Czochralski method for growing high quality ruby crystals. The resultant crys als normally displayed high crystallographic perfection as determined by x-ray and petrographic studies. Optical quality was primarily a function of the Cr_2O_3 concentration gradients that occurred. Problems still remaining are Cr_2O_3 variations, misorientation and residual strain.

4.0 EXPERIMENTAL PROCEDURE

The vapor train and furnace assembly designed for these crystal growth studies is shown schematically in Fig. 1. Reactant gases, chlorine (99.5% purity), pre-purified hydrogen (99.9%), carbon dioxide (99.5%) and C. P. carbon monoxide (99.5%) were passed through anhydrous calcium sulfate drying tubes. Hydrogen was also passed through a catalytic purifier to remove oxygen. All gases were then passed through flow meters and into the reaction chamber via a concentric or multiple-tube injector.

To generate a source of aluminum chloride vapor, high purity aluminum metal was chlorinated in a temperature-controlled chamber. Aluminum chloride was formed according to the following reaction:

$$Al(s) + 3/2Cl_2(g) \rightleftharpoons AlCl_3(g) \qquad (2)$$

This method permitted direct control of aluminum chloride vapor rather than depending upon the sublimation of solid aluminum chloride as a function of temperature and vapor pressure.

Aluminum chloride, hydrogen and carbon dioxide, were flowed through the primary or center annular tube. For ruby growth, chlorine was passed through either a short, outer tube or a separate secondary tube into a boat containing chromium metal, forming chromium chloride vapor by the following reaction:

$$Cr(s) + 3/2Cl_2(g) \rightleftharpoons CrCl_3(g) \qquad (3)$$

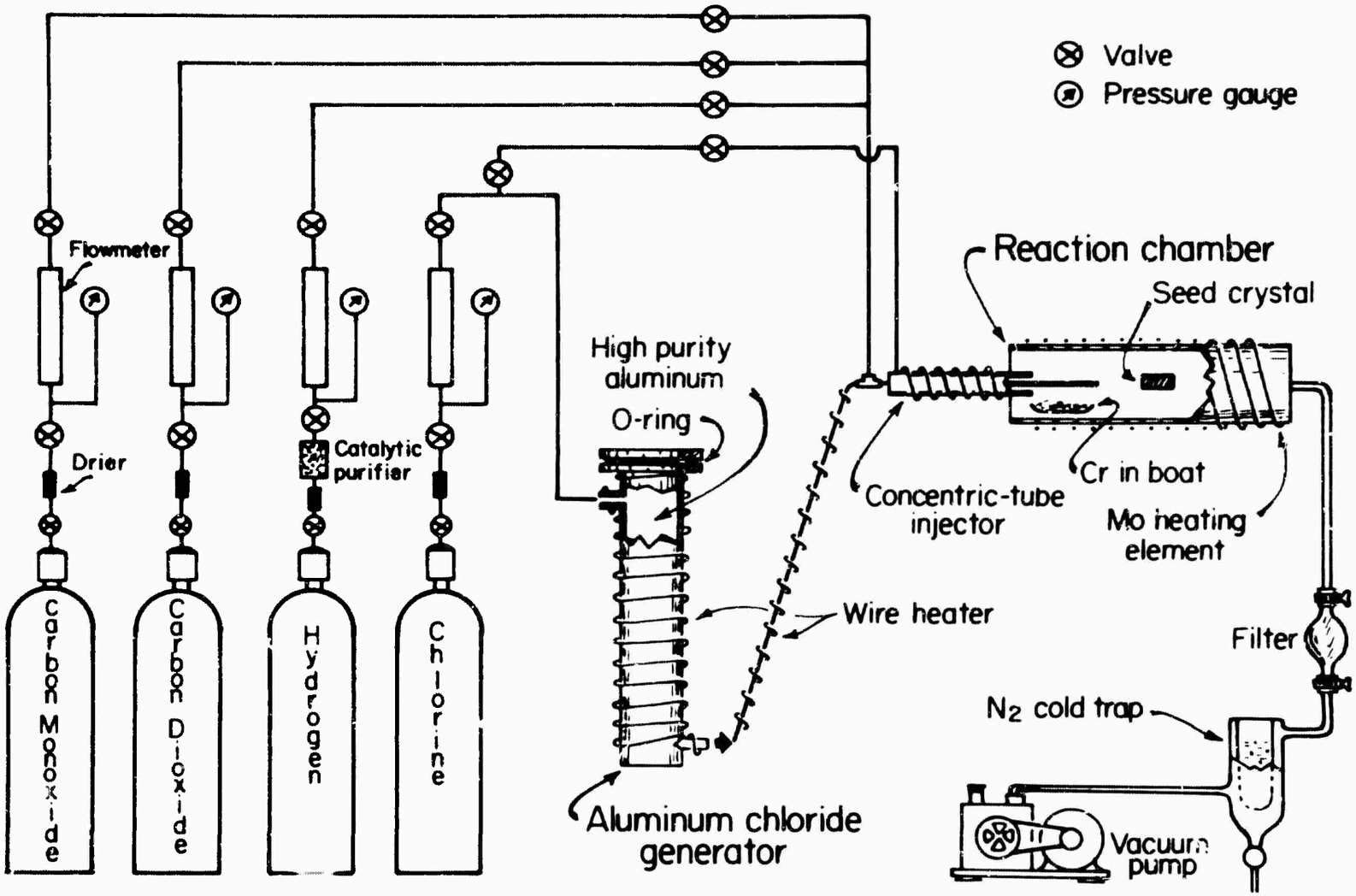

Figure 1: Schematic of Vapor Train and Furnace Assembly

Vapor growth was achieved in the isothermal reaction zone and the product gases of the chemical reaction, hydrogen chloride and carbon monoxide were exhausted through a filter and cold trap by means of a vacuum system. Ruby and sapphire crystals were formed by the reaction shown in equation (1) when $x > 0$ and $x = 0$, respectively. Hydrogen and carbon dioxide reacted to produce a controlled oxygen partial pressure, subsequently oxidizing chromium chloride and/or aluminum chloride simultaneously to form the desired crystalline variety. The overall reaction was a condensation process occurring at or near the substrate surface.

A 1-3/4 inch diameter molybdenum-element furnace operating at temperatures up to 1650°C was used for growth experiments. At the exhaust end of the reaction chamber, a sight port was located which permitted observation during crystal growth. Substrate temperature was measured with a calibrated optical pyrometer.

Investigations were conducted to relate the growth velocity (bulk crystal growth rate) of α-Al_2O_3 with the process parameters of vapor phase growth. These parameters included substrate temperature, total pressure, crystal orientation, reactant vapor velocity and partial pressures of reactant gases. A set of standard conditions was established permitting only one or a minimum number of growth variables during each growth experiment. Optimum conditions were established by correlating the growth velocities to process parameters.

Dislocation density, which is an indication of the degree of internal strain present in a crystal, was used as a measure of crystalline perfection. Chemical polishing and etching techniques[9,10] were utilized to reveal

dislocation structures for basal {0001} and prism $\{11\bar{2}0\}$ planes in sapphire and ruby crystals. The basal planes were chemically polished in 85% orthophosphoric acid (H_3PO_4) at 425°C for 150 seconds. Etching in potassium bisulfate ($KHSO_4$) at 675°C for 15-20 seconds developed triangular pits. The prism planes were chemically polished in potassium aluminum fluoride (K_3AlF_6) at 1000°C for 45 seconds. Polygonal etch pits were developed on these planes by etching in $KHSO_4$ at 675°C for 135 seconds. Prior to reagent immersion, samples were preheated to minimize thermal shock. Platinum crucibles were used to contain the heated etchants. Temperature measurement was achieved with platinum-platinum 10% rhodium thermocouples.

5.0 RESULTS AND DISCUSSIONS

5.1 Thermodynamic Considerations

Cr_2O_3 doped α-Al_2O_3 was formed from the vapor phase by the following general reaction:

$$(2-x)\,AlCl_3(g) + xCrCl_3(g) + 3H_2(g) + 3CO_2(g) \rightleftharpoons Cr_xAl_{2-x}O_3(s) + 3CO(g) + 6HCl(g) \quad (1)$$

The overall reaction actually consisted of the following simultaneous reactions in which $O_2(g)$, $Al_2O_3(s)$, $Cr_2O_3(s)$ and probably $Al_2O(g)$ as an intermediate product were formed.

$$2AlCl_3(g) + 3H_2(g) + 3CO_2(g) \rightleftharpoons Al_2O_3(s) + 3CO(g) + 6HCl(g) \quad (4)$$

$$2CrCl_3(g) + 3H_2(g) + 3CO_2(g) \rightleftharpoons Cr_2O_3(s) + 3CO(g) + 6HCl(g) \quad (5)$$

$$3CO_2(g) \rightleftharpoons 3CO(g) + 3/2O_2(g) \quad (6)$$

The equilibrium constant, K_p, of the overall reaction is represented by the following equation:

$$K_p = \frac{a_{Cr_xAl_{2-x}O_3}\, p_{CO}^3\, p_{HCl}^6}{p_{AlCl_3}^{2-x}\, p_{CrCl_3}^{x}\, p_{CO_2}^3\, p_{H_2}^3} \quad (7)$$

where a = activity (assumed to be unity) and

p = partial pressure.

Since the standard free energies of formation of each of the constituents in the preceding equation are known[12,13], the standard free energy change and equilibrium constant of the reaction were calculated and tabulated in Table I. A Cr_2O_3 dopant concentration of 0.10 w/o (1000 ppm) was used in the calculations.

The free energy change is highly negative at each temperature and becomes more negative with increasing temperature. Also, the equilibrium constant is far greater than unity at each temperature, both indicating that the reaction is favorable to proceed as written over the entire temperature range. However, the reaction was not readily observable at low temperatures due to an associated low reaction rate. The reaction rate was also controlled at high temperatures by the addition of specific amounts of product gases, carbon monoxide and hydrogen chloride, which suppressed the rate of formation of the solid oxide.

A substrate temperature greater than 1150°C was necessary to form an appreciable amount of alpha-alumina. The minimum temperature necessary for the formation of chromium chloride vapor (from solid chromium and chlorine gas) was 947°C, and a minimum temperature of 180°C was required to form gaseous aluminum chloride (from solid aluminum and chlorine gas).

TABLE I

Determination of Free Energy and Equilibrium Constant vs. Temperature for the Reaction:
$(2-x)\ AlCl_3(g) + xCrCl_3(g) + 3H_2(g) + 3CO_2(g) \rightleftharpoons Cr_xAl_{2-x}O_3(s) + 3CO(g) + 6HCl(g)$
(for x = 1000 ppm). ΔF° in Kcal./mole.

Temp. °K	Temp. °C	$-\Delta F^\circ$ $Cr_xAl_{2-x}O_3$	$-3\Delta F^\circ$ CO	$-6\Delta F^\circ$ HCl	$-2\Delta F^\circ$ $(1-x)AlCl_3$	$-\Delta F^\circ$ $xCrCl_3$	$-3\Delta F^\circ$ CO_2	$-\Delta F^\circ$ Reaction	Log K	K
500	227	361.98	113.10	139.8	287.71	.035	283.17	43.97	19.23	2.87×10^{19}
800	527	339.56	131.04	142.5	280.52	.030	283.62	46.95	13.38	2.40×10^{13}
1000	727	324.50	143.82	144.3	274.53	.026	283.63	54.23	11.87	7.42×10^{11}
1200	927	308.69	156.45	146.1	266.13	.023	283.98	61.11	11.13	1.35×10^{11}
1400	1127	293.00	168.93	147.9	257.74	.022	284.07	68.00	10.61	4.08×10^{10}
1500	1227	285.29	175.11	148.8	253.55	.022	284.13	71.50	10.41	2.57×10^{10}
1600	1527	263.10	193.44	151.5	240.96	.022	284.16	82.90	10.08	1.20×10^{10}
2000	1727	246.70	205.53	153.0	233.77	.022	284.16	87.28	9.55	3.56×10^{9}

5.2 Kinetic Considerations

Bulk crystal growth rate of α-Al_2O_3 plotted as an inverse logarithmic function of the substrate temperature yielded a straight line as shown in Fig. 2. This suggests that the vapor growth process, condensation of a supersaturated vapor, is a first order reaction and can be represented by the Arrhenius relationship:

$$G = G_o \exp(-Q/RT) \tag{8}$$

where G = bulk crystal growth rate (mg/cm^2-hr)

G_o = growth constant

Q = experimental activation energy of the growth process

R = molar gas constant (1.99 cal/mole)

T = absolute temperature (°K)

The experimental activation energy, Q, is 3.25 ev (74,930 cal/mole). In order for crystal growth to occur by gaseous diffusion, the growth rate must vary as $T^{3/2}$ (Ref. 14). Since the data do not obey this relationship, it is suggested that another mechanism may be involved in the condensation process.

The kinetics of the overall process for the transfer of material during condensation from a supersaturated vapor involve (a) transport of reactant vapors to the substrate-vapor boundary layer, (b) reaction at this boundary layer, that is, deposition on the substrate and (c) transport of gaseous products away from this layer.

At the elevated substrate temperatures in the growth of α-Al_2O_3, it seems likely that the rate controlling process is the diffusion of material across the substrate-vapor boundary layer. The degree of supersaturation

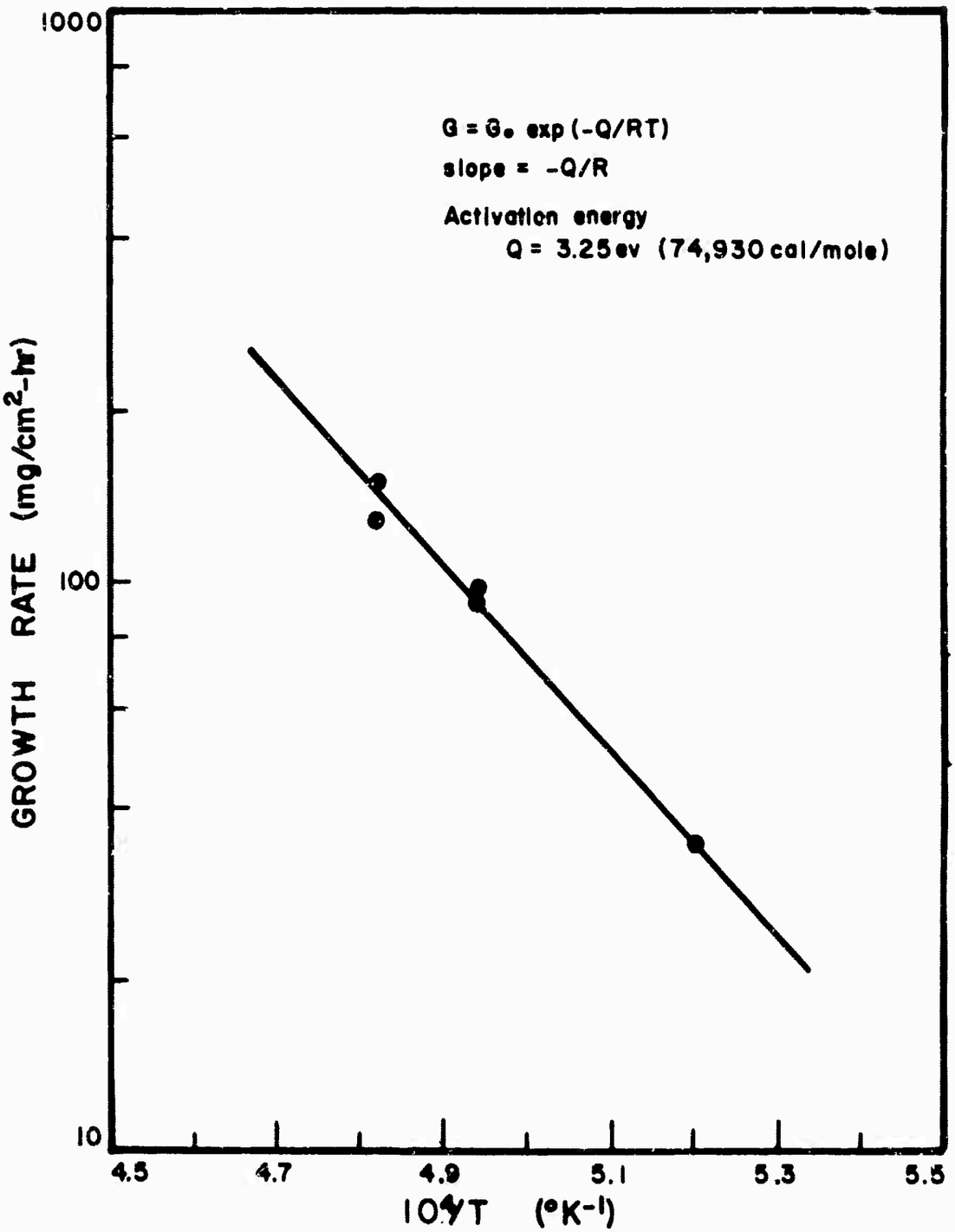

Figure 2: Bulk Crystal Growth Rate vs. 1/T

determines the morphological species formed. Under conditions where bulk crystal growth is favorable and homogeneous nucleation is minimized, increasing the velocity and subsequently the Reynolds number to an optimum value, the growth rate will increase as the rate at which the reactant gases reach the substrate and diffusion of material across the substrate is increased.

To determine the type of flow existing in the growth zone, the Reynolds number, N_{re}, was calculated:

$$N_{re} = \frac{dv}{\mu} \tag{9}$$

where d = diameter of growth zone (cm)

v = velocity of reactant vapor stream (cm/sec)

μ = kinematic viscosity = $\frac{\nu \text{ (viscosity)}}{\rho \text{ (density)}}$ = stokes

Under the standard growth conditions, the velocity in the growth zone was calculated as follows:

$$v_{STP} = \frac{(1{,}907 \text{ cm}^3/\text{min})}{(60 \text{ sec/min})\ (15.8 \text{ cm}^2)} = 2.01 \text{ cm/sec}$$

$$v(1750^\circ\text{C},\ 9.0 \text{ torr}) = (v_{STP})\ (T[^\circ\text{K}]/293)\ (760/P[\text{torr}] = 1{,}173 \text{ cm/sec}$$

$$\mu = \frac{\nu}{\rho} = \frac{5.46 \times 10^{-4} \text{ poise}}{1.46 \times 10^{-6} \text{gm/cm}^3} = 3.90 \times 10^2 \text{ stokes}$$

$$N_{re} = \frac{dv}{\mu} = \frac{(4.5 \text{ cm})\ (1.173 \times 10^3 \text{cm/sec})}{(3.90 \times 10^2 \text{gm-cm}^3/\text{sec-gm-cm})} = 13.5$$

For this approximate value of N_{re} based upon the average velocity, laminar flow exists, i.e., molecular vapor flow occurs parallel to the longitudinal axis of the furnace chamber without an appreciable radial component. At high N_{re} values, approximately 2×10^3, the flow would be turbulent due to the existence of vortexes or eddy currents in the growth zone. Increasing the Reynolds number above 13.5 would increase the transport of material across the substrate-vapor boundary; however, from velocity measurement studies, the bulk crystal growth rate would decrease.

5.3 Growth Velocity vs. Reactant Gas Velocity

At a temperature of 1750°C, total pressure of 9.0 torr and constant partial pressure ratios of the reactant gases α-Al_2O_3 vapor growth velocity (bulk crystal growth rate) was measured using 60° α-Al_2O_3 rod substrates. A range of velocities was obtained by varying the flow rates of the reactant gases and maintaining a constant total pressure by throttling the vacuum pumping system.

Figure 3 shows the rate of bulk crystal growth as a function of average reactant vapor velocity and total pressure. For laminar flow, the shape of the velocity-distribution curve is parabolic; therefore, the velocity at the center of the tube where bulk crystal growth occurs is twice the average velocity. The growth rate varied from negligible growth at a velocity of 300 cm/sec to a maximum at approximately 1170 cm/sec and decreased with increasing velocity. The low growth rate at lower velocities was attributed to deposition on the furnace walls prior to the reactant gas stream reaching the substrate. At very high velocities, the short gas residence time suppressed kinetic

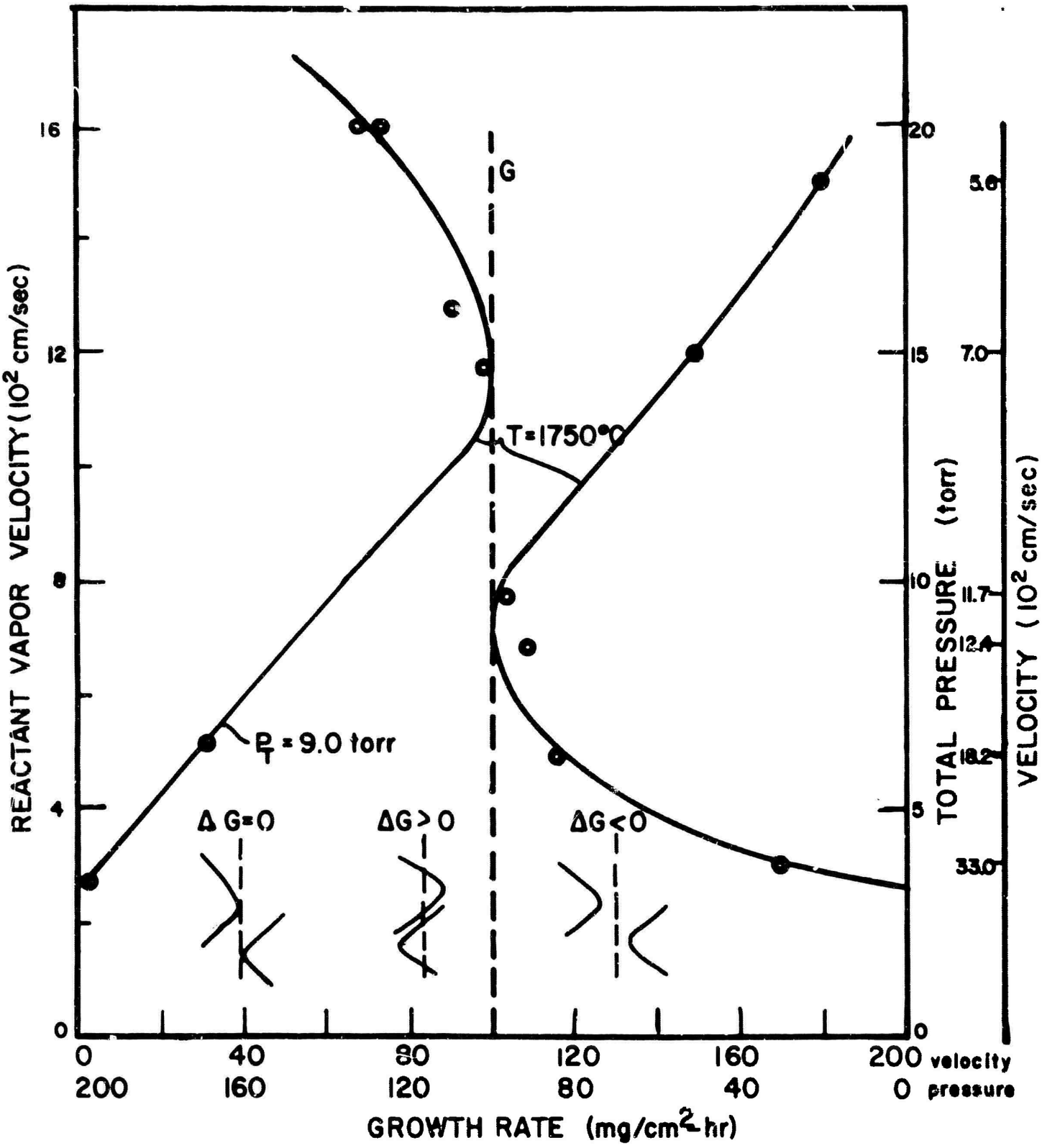

Figure 3: Growth Rate of α-Al_2O_3 vs. Reactant Vapor Velocity and Total Pressure (constant reactant gas partial pressure ratios, temperature).

processes which caused growth to proceed by material transport across the substrate-vapor boundary.

A vertical line, G, was drawn at a growth rate of 100 mg/cm^2-hr. which represents the maximum observed rate at 1750°C. This rate was established as $\Delta G = 0$. Higher growth rates as related to velocity, total pressure and temperature would be represented as $\Delta G > 0$ while lower growth rates would be represented as $\Delta G < 0$.

5.4 Growth Velocity vs. Total Pressure

Also represented in Fig. 3, the bulk crystal growth rate of α-Al_2O_3 was measured as a function of total pressure at a temperature of 1750°C and constant partial pressures. The total pressure was varied by throttling the vacuum pumping system. At low pressures (high velocities), very short gas residence times resulted in low growth rates. Maximum growth occurred at a total pressure of approximately 9.0 torr (velocity = 1170 cm/sec). At higher pressures (lower velocites) which increased the residence time, deposition on the furnace walls may have increased which decreased crystal growth. Also, at higher pressures, the supersaturation increased which favored homogeneous nucleation and decreased crystal growth. These homogeneously nucleated powders were submicron particles of alumina[15] (0.05 microns diameter in 1 micron agglomerates).

5.5 Growth Velocity vs. Substrate Temperature

In Fig. 4, the growth rate is shown as a function of substrate temperature at constant total and partial pressures. At 1550°C, little bulk crystal growth occurred, although whisker and fiber formation were abundant. Growth

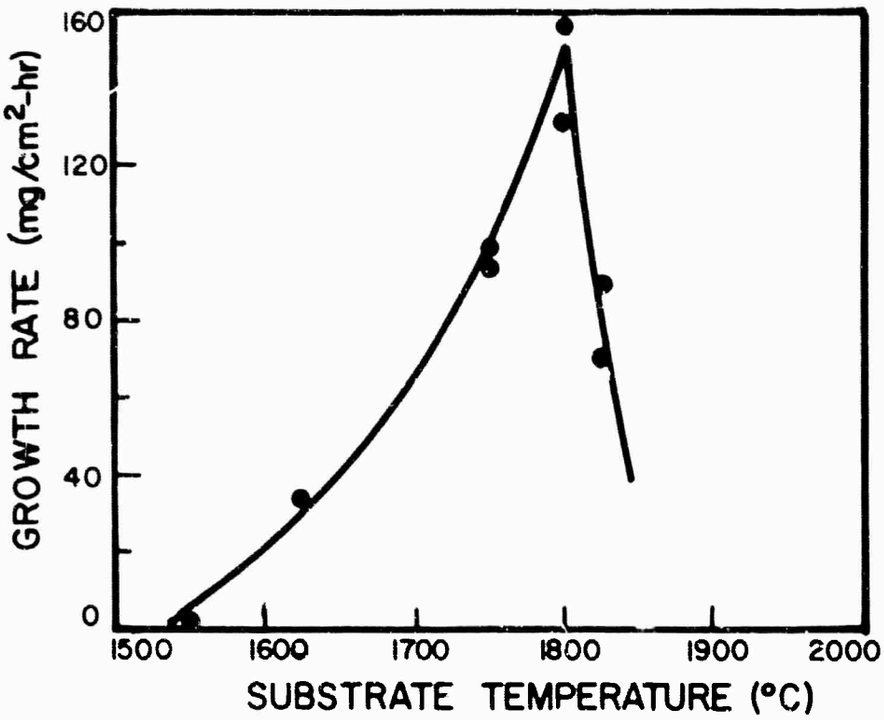

Figure 4: Growth Rate of α-Al_2O_3 vs. Substrate Temperature (constant total pressure, reactant gas partial pressures).

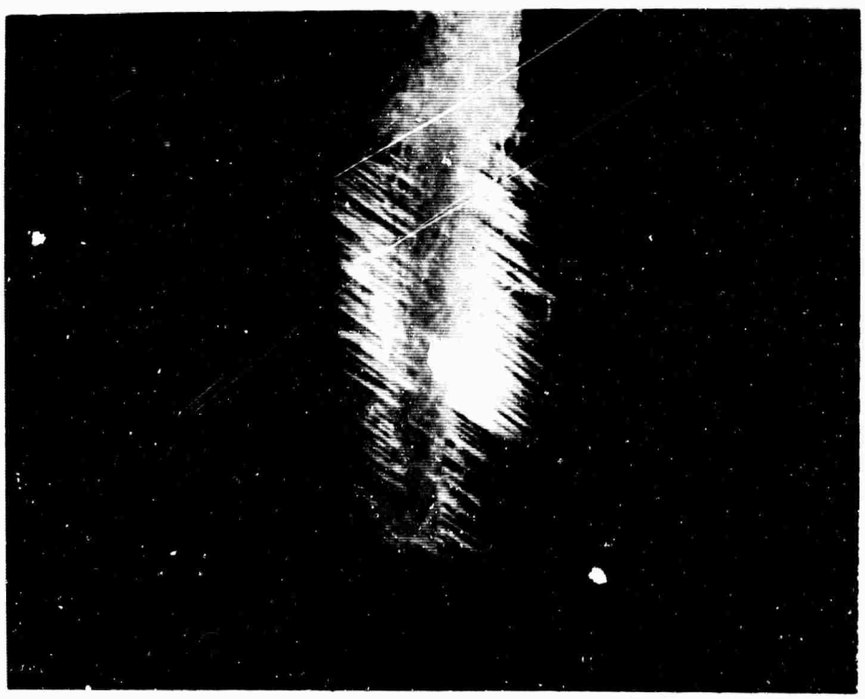

Figure 5: Single Crystal α-Al_2O_3 Fibers on 60° Orientation Sapphire Substrate. 2.1x.

rate was maximum at 1600°C. From free energy determinations discussed previously, ΔF_R° became more negative with increasing temperature indicating that the overall reaction (1) became more favorable. From kinetic considerations, the rate of reaction was greater with increasing temperature; therefore, above 1600°C the lower growth may be attributed to two factors. The first is that the rate of evaporation of Al_2O molecules from the substrate surface is greater than the rate of condensation. Secondly, because of the higher temperature at essentially uniform reactant gas velocities, depletion of the reactant vapor stream may occur by increased deposition on the furnace walls.

The growth rates shown in Fig. 3 were measured on crystals grown at a constant substrate temperature of 1750°C. Since the growth rate is maximum at 1600°C, rate measurements made at this temperature would result in $\Delta G > 0$, indicating more favorable conditions for bulk crystal growth. Growth rates below those obtained at 1750°C would result in $\Delta G < 0$.

Figure 5 shows single crystal sapphire fibers grown on a 60° sapphire substrate. These fibers grew with preferred orientations up to 0.008 inch diameter and 0.5 inch long in two hours, although they began as whiskers which formed in minutes after a brief induction period. Lowering the temperature changed the degree of supersaturation to the region where fiber growth was favorable and bulk crystal growth was negligible.

5.6 Growth Velocity vs. Reactant Gas Partial Pressures

Growth velocity was measured as a function of aluminum chloride partial pressure (p_{AlCl_3}) as shown in

Figure 6 (constant p_T, T, p_{H_2}, p_{CO_2}, p_{CO}). A slight modification of reactant vapor velocity resulted from varying p_{AlCl_3}. It is seen that growth rate increased with an increase in p_{AlCl_3} as additional aluminum became available for the overall reaction. After a maximum was reached, the bulk crystal growth rate decreased with a further increase in p_{AlCl_3}. This is attributed to an increase in supersaturation with an accompanying rise in homogeneous nucleation, resulting in excess sub-micron alumina particle formation. Therefore for the present system, p_{AlCl_3} = 0.51 torr ($AlCl_3$ flow rate = 0.12 lpm) was found to be optimum.

Figure 7 shows the bulk crystal growth rate as a function of the ratio of hydrogen partial pressure to carbon dioxide partial pressure. Total pressure, substrate temperature and partial pressures of aluminum chloride, carbon dioxide and carbon monoxide were held constant, while partial pressure of hydrogen and changes in velocity were the only variables. The growth rate increased continuously with higher hydrogen/carbon dioxide up to a ratio of 7:1 where the gas velocity was 1540 cm/sec. It was shown in Fig. 3 that increasing the velocity above 1170 cm/sec (under described conditions) resulted in a decrease in growth rate. The partial pressure ratio may be more of a contributing factor to reaction completion than the velocity. From Fig. 5 it appears that the p_{H_2}/p_{CO_2} limit may have been approached. The increased growth rate achieved by increasing the hydrogen partial pressure may be attributed to excess hydrogen reaction with chlorine forming hydrogen chloride, further driving the overall reaction to completion.

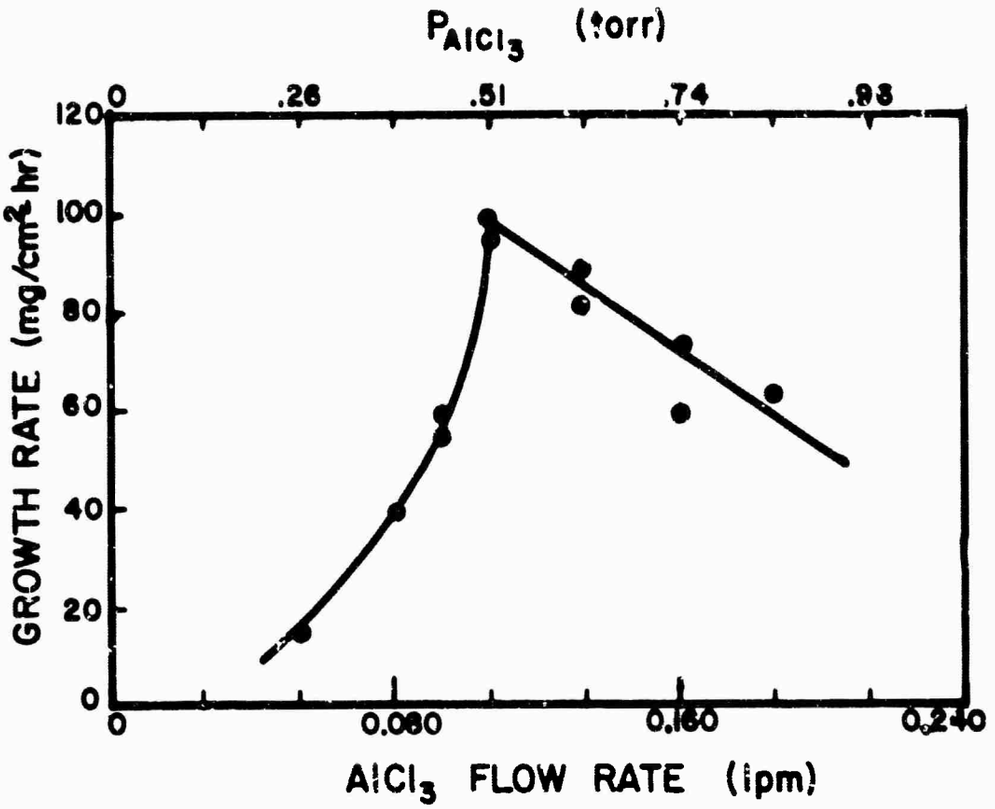

Figure 6: Growth Rate of α-Al_2O_3 vs. Aluminum Chloride Partial Pressure (constant P_T, T, P_{H_2}, P_{CO_2}, P_{CO}).

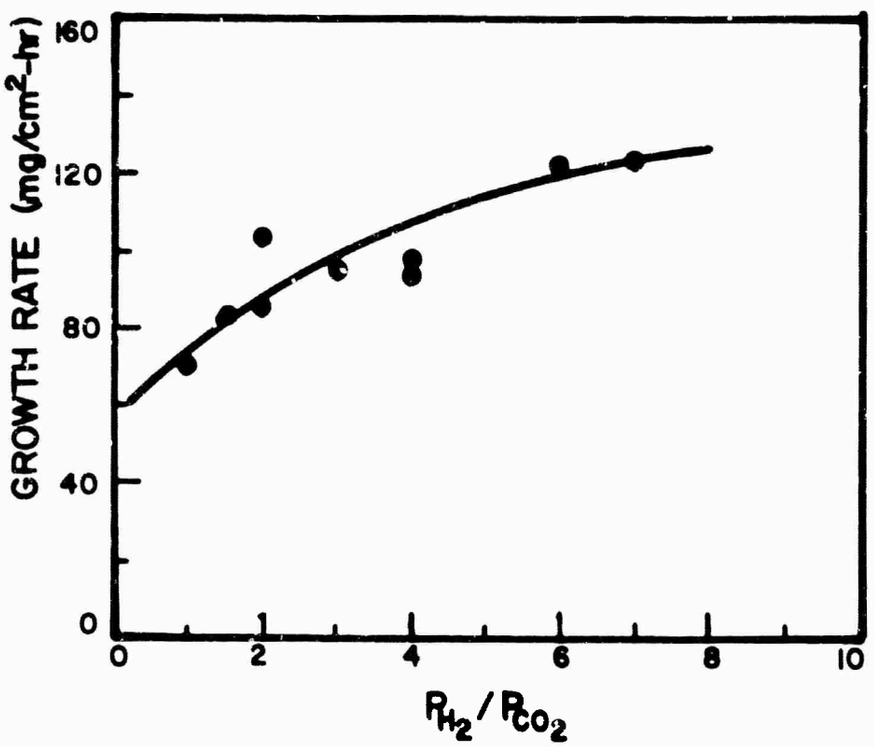

Figure 7: Growth Rate of α-Al_2O_3 vs. P_{H_2}/P_{CO_2} (constant P_T, T, P_{AlCl_3}, P_{CO_2}, P_{CO}).

5.7 Growth Velocity vs. Orientation

Growth velocity was measured as a function of crystallographic orientation utilizing flame-fusion grown, spherical α-Al_2O_3 substrates. The spheres were mounted on the end of a sapphire rod in the radial center of the growth zone oriented with the {0001}plane perpendicular to the reactant gas flow. Figure 8 shows a substrate and vapor-grown crystals after growth of 1-1/2, 3, 6, and 12 hours, respectively, at constant supersaturation, substrate temperature, total pressure, reactant gas velocity and reactant gas partial pressures. The existence of three distinct sets of crystallographic planes was determined by optical goniometry methods in the vapor-grown crystals. These were two basal planes {0001} (in the plane of the photograph), six prism planes $\{11\bar{2}0\}$ (perpendicular to the plane of the photograph) and two sets of six planes each between the basal and prism planes, which appear to be either $\{22\bar{4}3\}$ or $\{11\bar{2}2\}$ planes. Exact determination of these latter planes was difficult due to the development of vicinal faces during growth. Also, in the twelve-hour crystal, one set of these planes completely grew itself out of existence. The fastest growth directions (perpendicular to the aforementioned planes) were the rhombohedral $[10\bar{1}1]$ and prism $[10\bar{1}0]$ directions which grew 2.61 (0.0188 in/hr) and 1.46 (0.0095 in/hr), respectively, times faster than the slowest growing "c"-direction [0001] (0.0072 in/hr). Frequently, secondary nucleation occurred on the {0001} plane directly perpendicular to the impinging reactant vapor stream.

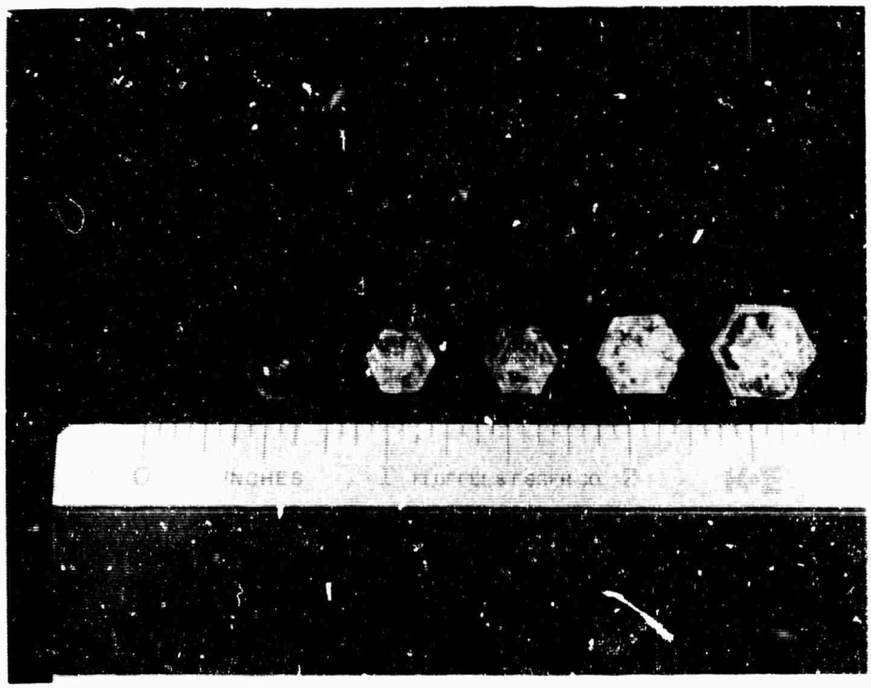

Figure 8: Spherical Substrate and Vapor-Grown Sapphire Crystals Grown for 1 1/2, 3, 6 and 12 hours, Respectively, for Orientation Studies. 1.28x.

5.8 Crystal Growth

Ruby crystals were grown epitaxially up to a weight of 90.7 grams in 52 hours (1.74 gm/hr). Subsequent machining operations were performed on the as-grown crystals without annealing procedures. Fracture did not occur which was attributed to the low residual strain in the crystals. Figure 9 shows several 60° ruby monocrystals of controlled Cr_2O_3 concentrations vapor grown at various growth velocities. Some voids were observed in the 60° crystals which emanated at the flame fusion substrate. They extended into the vapor overgrowth only in the fastest growth directions perpendicular to the 60° longitudinal axis and were attributed to defects on the substrate surface.

Ruby crystals of 0° orientation grown under the same growth parameters as the 60° crystals shown in Fig. 9 tended to become polycrystalline. Some 0° crystals also developed thermal cracks in the substrate which propagated through the vapor overgrowth; however, more moderate growth rates and slower heating and cooling cycles overcame these problems. Ruby monocrystals were grown with up to 4.1 w/o Cr_2O_3(2.8 w/o Cr) concentrations demonstrating the capability of the vapor phase doping procedure.

In the ruby crystals depicted in the aforementioned figure, chromium chlorination temperatures were partially below the $CrCl_3$ boiling point. This resulted in partial solid $CrCl_3$ formation which obstructed chlorine flow. This in turn generated non-uniform $CrCl_3$ vapor flow which produced radial Cr_2O_3 concentration gradients. Using higher chlorination temperatures to eliminate $CrCl_3$(s) formation and closer substrate temperature control would favor uniform Cr_2O_3 concentration.

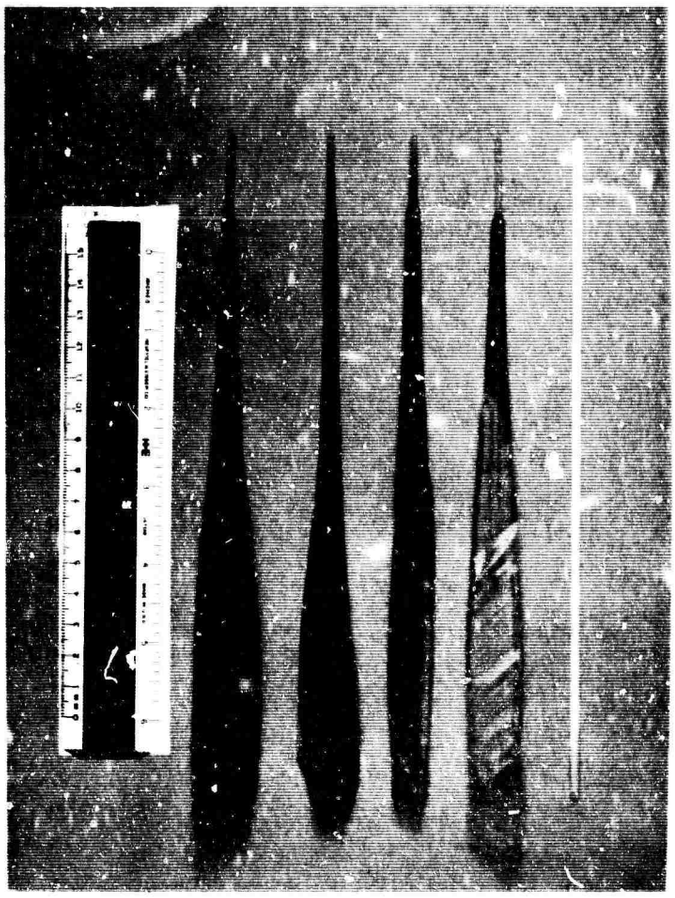

Figure 9: 60° Orientation Vapor-Grown Ruby Monocrystals Grown at Various Growth Velocities. (From left to right), (a) 90.7 gm (52 hrs), (b) 43.1 gm (30 hrs), (c) 39.8 gm (30 hrs), (d) 77.6 gm (47 hrs), (e) 60° Flame-Fusion Grown Substrate.

It appears desirable to maintain a sufficiently high substrate temperature since the rate of nucleation decreases with increasing temperature, thus the growth layers form from fewer nuclei. Also at higher temperatures absorbed atoms have higher mobility which favor higher crystalline perfection.

Discontinuous reactant gas flow resulted in the formation of boundary layers although continuous single crystal growth was produced. Figure 10 shows three intermittent cycles of ruby overgrowth on a 60° sapphire substrate. Boundary layers are seen at three stages of growth: in each cycle reactant gas flows were stopped and then continued after a given time interval. This was attributed to layers of higher chromium concentration caused by different condensation and deposition rates of Al_2O_3 and Cr_2O_3 and instantaneous differences in supersaturation as each new layer was deposited. Continuous vapor flow produced continuous monocrystals with no boundary layer formation.

5.9 Dislocation Density

Figure 11 shows the prism plane $\{11\bar{2}0\}$ of an α-Al_2O_3 flame-fusion grown substrate with vapor overgrowth of ruby in the upper portion. Sub-boundaries extended into the overgrowth from the substrate. The dislocation density of the substrate was 4.9×10^6 dislocations/cm^2 compared to 6.2×10^5/cm^2 for the ruby overgrowth. Ruby specimens[16] (0.30 w/o Cr_2O_3) showed an increase of 25 percent in dislocation density compared to sapphire, both flame-fusion grown. However, there was a reduction of 87.5 percent from the substrate to the ruby overgrowth in the aforementioned

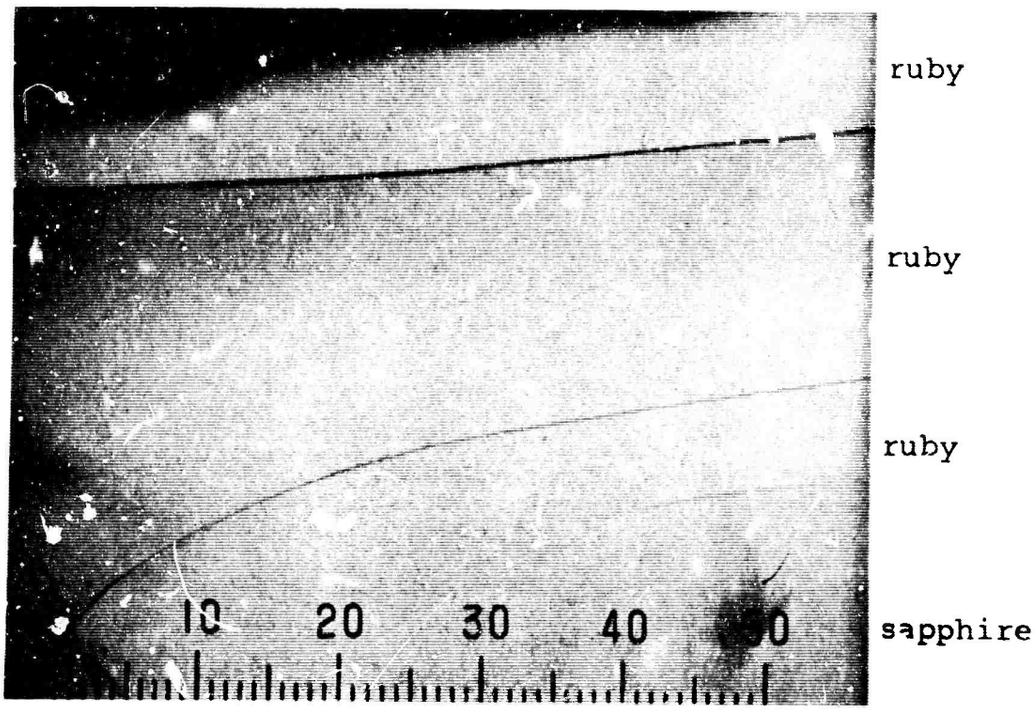

Figure 10: Three Intermittent Cycles of Ruby Overgrowth on 60° α-Al_2O_3 Substrate. 93x.

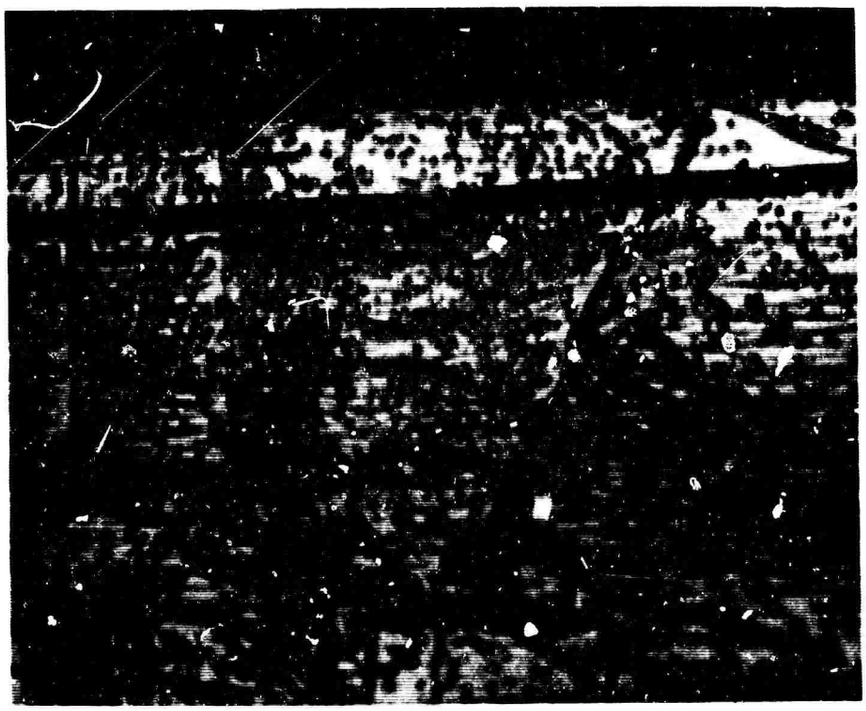

Figure 11: Etch Pits on {1120} Plane of α-Al_2O_3 Substrate (bottom) and Cr_2O_3-Doped α-Al_2O_3 Vapor Overgrowth (top). 200x.

figure. The basal plane {0001} dislocation density of a typical "c" axis vapor-grown platelet of $3.6 \times 10^3/cm^2$ is shown in Fig. 12. Dislocation densities as low as $13/cm^2$ were measured on large vapor-grown α-Al_2O_3 platelets (Fig. 13). A total of only eight pits was detected on the entire surface area of this platelet. The density of this maximum area was $2.3 \times 10^3/cm^2$. Dislocation density tended to decrease with increasing thickness of vapor overgrowth. Vapor-grown crystals generally exhibited a density reduction of one to three orders of magnitude over their flame-fusion substrates.

5.10 Crystalline Purity

Ruby crystals were grown with total impurity levels determined by spectrochemical analysis as low as 4 ppm (Table II). Source materials used for these growth studies were high purity aluminum and chromium, prepurified hydrogen, welding carbon dioxide, C. P. carbon monoxide and chlorine. The analysis of these source materials is shown in Table III. Other potential impurity sources were the alumina furnace tube injector system and vapor train.

The vapor growth technique provided an overall purification-type action from differential chlorination and distillation. Impurity elements in the aluminum and chromium exhibited different kinetic behavior under the existing pressure and temperature conditions. Some impurities may have remained in the halide generators because of low chlorination rates and/or low vapor pressure. Others may have passed into the growth chamber where they displayed different thermodynamic stabilities from $AlCl_3(g)$ and $CrCl_3(g)$.

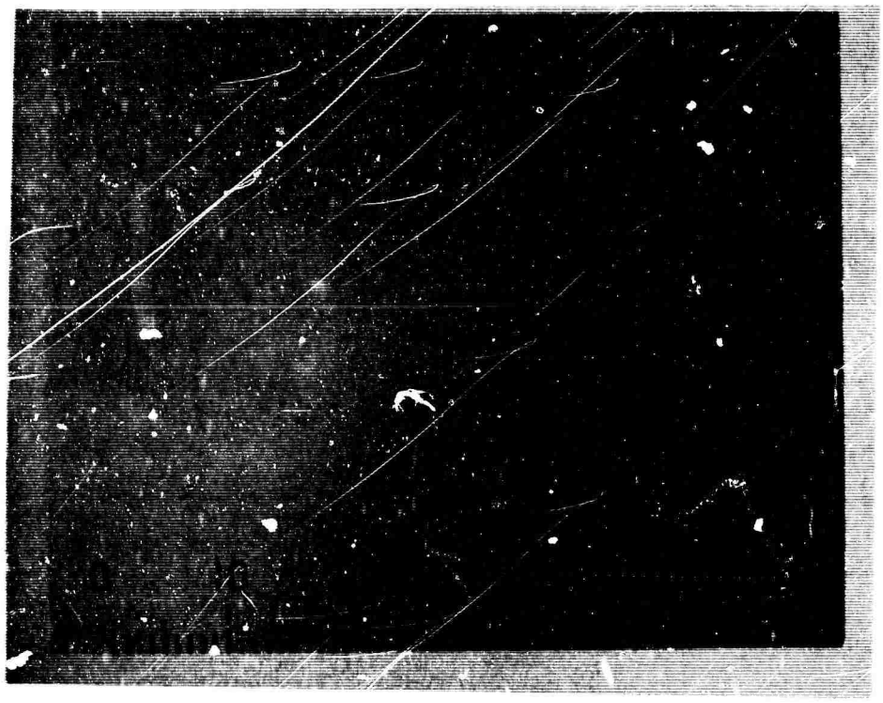

Figure 12: Etch Pits on {0001} Plane of Small Vapor Grown α-Al_2O_3 "c" Axis Platelet. Dislocation Density 3.8 x $10^3/cm^2$. 186x.

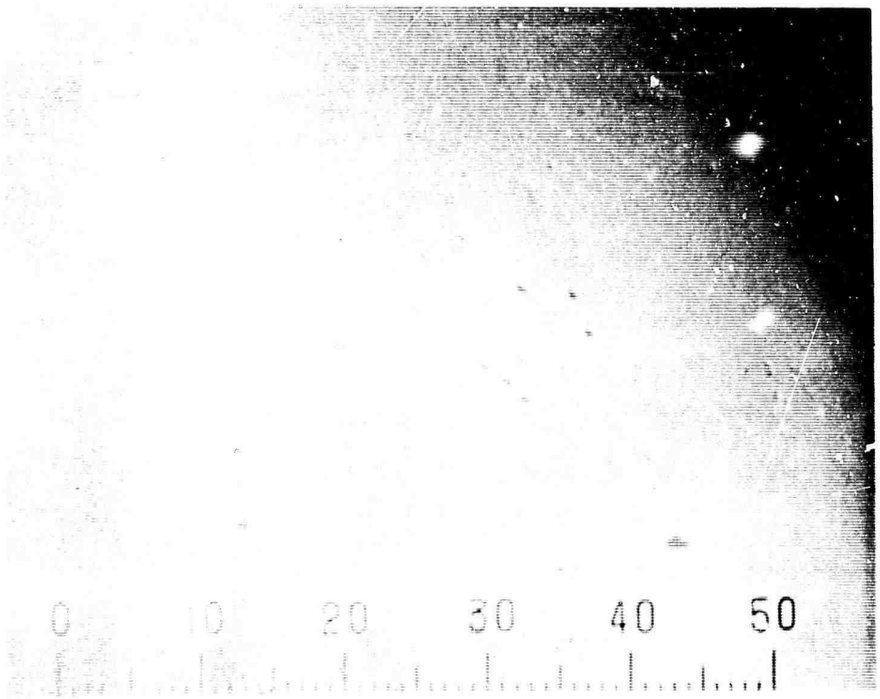

Figure 13: Etch Pits on {0001} Plane of Large Vapor Grown, "c" Axis α-Al_2O_3 Platelet. Only Eight Pits Detected on Entire Crystal. Dislocation Density 13/cm^2. (This maximum area 2.3 x $10^3/cm^2$). 186x.

TABLE II

Spectrochemical Analysis of Vapor-Grown Ruby Crystal (#R-15)

Element	ppm
Na	1-10
Mg	<1
Si	1-10
Ag	<1

All other elements not detected.

TABLE III

Analysis of Source Materials Used in Vapor Growth of High Purity Ruby Monocrystals (ppm)

Aluminum: Mg-20, Zn-8, Fe-3, Cd-2, Si-2, Cu-1, Ag <1

Chromium: Si-2, Mg < 1

Prepurified H_2: 99.9% min. purity, < 20 ppm O_2, dew point < -75°F,

Typical Analysis: O_2 -8, N_2 -400, CO and CO_2 < 1, hydrocarbons -1, Cl_2-1, dew point -95°F

C. P. Grade CO: 99.5% min. purity, CO_2 - 200, O_2 - 20, N_2 -75, dew point -60°F.

Welding Grade CO_2: 99.5% min. purity, N_2 -3400 ppm max., O_2 - 900 max., H_2O -700 max.

Chlorine: min. purity 99.5%, 66 ppm residue.

Also, impurity atoms that impinged in the substrate may have volatilized rather than become incorporated into the crystalline matrix.

6.0 CONCLUSIONS

1. A vapor train, furnace assembly and related apparatus were designed and constructed for the vapor phase growth of oriented ruby and sapphire monocrystals.
2. Ruby monocrystals were grown up to a weight of 90.7 grams in 52 hours.
3. The variables which influence the formation kinetics of the overall reaction were investigated. These included substrate temperature, total pressure, orientation, gas velocity and reactant gas partial pressures.
4. Thermodynamic calculations indicated that the formation of ruby and sapphire were favorable over the temperature range 227°-1727°C (500°-2000°K) and became more favorable with increasing temperature.
5. Control of the overall reaction process was qualitatively determined to result from control of reaction kinetics.
6. Determination of activation energy suggested that a mechanism other than gaseous diffusion controls crystal growth.
7. The fastest growth directions in α-Al_2O_3 were the rhombohedral $[10\bar{1}1]$ and prism $[10\bar{1}0]$ directions which grew 2.61 and 1.46, respectively, times faster than the slowest growing "c" [0001] direction.
8. Machining operations were performed on the as-grown crystals without annealing treatments. Fracture did not occur which was attributed to the low residual strain in the crystals.

9. Some voids were observed in 60° crystals which emanated at the flame-fusion substrate and extended into the vapor overgrowth only in the fastest growth directions.
10. Ruby monocrystals were grown with up to 4.1 weight percent Cr_2O_3.
11. Radial Cr_2O_3 concentration gradients were present in ruby monocrystals which still must be overcome to obtain laser quality crystals.
12. Dislocation density tended to decrease with increasing thickness of vapor overgrowth.
13. Vapor-grown crystals generally exhibited a dislocation density reduction of one to three orders of magnitude over their flame-fusion substrates. Densities as low as $13/cm^2$ were measured on large vapor-grown α-Al_2O_3 platelets.
14. Ruby crystals were grown with total impurity levels determined by spectrochemical analysis as low as 4 ppm.

7.0 REFERENCES

1. Schaffer, P. S., "Vapor Phase Growth of Alpha-Alumina Single Crystals", Accepted for Publication in J. Amer. Cer. Soc.

2. Jack, K. H. and Stephenson, G. W., "The Vapor-Phase Production of Refractory Oxide Crystals", presented at C.V.D. Electronic Materials Research Conference, University College of North Wales, Bangor, England, (1962).

3. Van Houten, G. R., White, J. F. and Botje, J. M., "Formation of Alumina Coatings on Beryllia by a Vapor Deposition Process", General Electric Co., APEX-699, (1961).

4. Powell, C. F., Campbell, I. E. and Gonser, B. W., Vapor Plating, J. Wiley & Sons, (1955).

5. Battelle Memorial Institute, "The Growth of Ruby Crystals Under High-Pressure Hydrothermal Conditions", ARPA, Final Report, (1963).

6. White, E.A.D., and Hayward, R.J.R. and Brown, C.S. "Crystals for Masers", C.V.D. Research Project RP3/27, Second Progress Report, General Electric Co., Ltd., Wembley, England, (1961).

7. Lambdin, R. W., "Hydrothermal Growth of Large Ruby Single Crystals", Interim Progress Report, ASD Project No. 8-132, Airtron, Division of Litton Ind., (1963).

8. Miller, J. F., Miller, S. E. and Goering, H. L., "Growth of Ruby Crystals from Solution", Final Technical Report, Contract Nonr-3822(00), May, 1964.

9. Nestor, O. H., "Czochralski Ruby", Annual Summary Report, Contract Nonr-4132(00), AD443-460, (1964).

10. Scheuplein, R. and Gibbs, P., "Surface Structure in Corundum: 1, Etching of Dislocations", J. Am. Cer. Soc., 43, (9), 458-471, (1960).

11. Alford, W.J. and Stephens, D.L., "Chemical Polishing and Etching Techniques for Al_2O_3 Single Crystals", J. Am. Cer. Soc., 46, (4), 193-194 (1963).

12. Coughlin, J.P., "Contributions to the Data on Theoretical Metallurgy", Bureau of Mines, Bulletin 542, (1954).

13. Glassner, A., "The Thermochemical Properties of the Oxides, Fluorides and Chlorides to 2500°K", ANL-5750, (1957).

14. Bird, R. B., Stewart, W.E. and Lightfoot, E.N., Transport Phenomena, Wiley & Sons, Inc., 510, (1960).

15. Campbell, W. B., "Feasibility of Forming Refractory Fibers by a Continuous Process", Seventh Quarterly Progress Report, Contract DA-19-020-AMC-0068(X), May, 1965.

16. Stephens, D. L. and Alford, W. J., "Dislocation Structures in Single Crystal Al_2O_3", J. Am. Cer. Soc., 47, (2), 81-86 (1964).

8.0 ACKNOWLEDGMENTS

The author is deeply appreciative of the valuable assistance given to him by W. B. Campbell and R. C. Folweiler, during the experimentation and writing of this report, and the experimental competence of L. G. Terrenzio, all of Lexington Laboratories, Inc.